ARTICLE OPEN

Check for updates

Spin memory of the topological material under strong disorder

Inna Korzhovska[1], Haiming Deng[1], Lukas Zhao[1], Yury Deshko[1], Zhiyi Chen[1], Marcin Konczykowski[2], Shihua Zhao[1], Simone Raoux[3] and Lia Krusin-Elbaum [1]✉

Robustness to disorder is the defining property of any topological state. The ultimate disorder limits to topological protection are still unknown, although a number of theories predict that even in the amorphous state a quantized conductance might yet reemerge. Here we report that in strongly disordered thin films of the topological material Sb_2Te_3 *disorder-induced spin correlations* dominate transport of charge—they engender a spin memory phenomenon, generated by the nonequilibrium charge currents controlled by localized spins. We directly detect a glassy yet robust disorder-induced magnetic signal in films *free of extrinsic magnetic dopants*, which becomes null in a lower-disorder crystalline state. This is where large isotropic negative magnetoresistance (MR)—a hallmark of spin memory—crosses over to positive MR, first with only one e^2/h quantum conduction channel, in a weakly antilocalized diffusive transport regime with a 2D scaling characteristic of the topological state. A fresh perspective revealed by our findings is that spin memory effect sets a disorder threshold to the protected topological state. It also points to new possibilities of tuning spin-dependent charge transport by disorder engineering of topological materials.

INTRODUCTION

Electronic disorder[1] and elementary excitations in quantum condensed matter are fundamentally linked and it is well established that spatially fluctuating potentials tend to promote decoherence and localization of fermions, i.e., the formation of Anderson insulators[2]. The interplay of interactions and disorder often leads to new quantum behaviors; disorder typically boosts interparticle correlations both in charge and in spin channels, and that could either aid or suppress the motion of charge[3]. Spin effects related to disorder are particularly important when spin-orbit coupling (SOC) is strong[4], and when spin-dependent charge transport can be electrically manipulated for uses, e.g., in spin-based electronics[5].

Strong SOC is a hallmark of three-dimensional (3D) topological insulators[6], where 2D gapless spin-polarized Dirac surface states are robust against backscattering. Most topological materials are known to contain a natural population of charged defects[7] that do not cause a destruction of the topological Dirac states; indeed, they can be compensated[8], although Dirac puddle disorders[9] may remain. Under weak disorder, a coherent interference of electron waves survives disorder averaging[10], and strong SOC enhances conductivity by a quantum weak antilocalization (WAL) correction related to the topological π-Berry phase[6] when magnetic impurities are absent. With increasing disorder the 2D WAL channels can be outnumbered by the weak localization (WL) channels[11]—this is a precursor of Anderson localization[2], which occurs at strong disorder. Under strong disorder, theory and numerical simulations[12–14] predict an emergence of a new topological state, dubbed 'topological Anderson insulator', in which conductance $G_0 = e^2/h$ is quantized. Indeed, recent theoretical demonstrations of topological phases in amorphous systems[15] point to promising new possibilities in engineered random landscapes. Strong disorder, however, is not trivial to install, quantify and control, and topological matter under such conditions has not yet been experimentally tested.

Here we implement an extensive range of site disorder—from amorphous to crystalline state—in Sb_2Te_3, the material which is a known second generation topological insulator[16,17], and report that under strong structural and electronic disorder conditions dynamic spin correlations dominate charge transport over a surprisingly large range of magnetic fields. These correlations imprint spin memory on the electrons hopping via localized spin sites. Predicted to be small[18] and thus practically unobservable in the conventional materials, the effect found here is large; it persists over a surprisingly wide range of disorder and well within the disordered crystalline topological phase, as long as variable range electron hopping (VRH)[19] is at play. It eventually transitions into the characteristic 2D WAL regime when a conductance channel quantized to $G_0 = e^2/h$, characteristic of the topological state, is established. The spin memory uncovered in this work is *not an orbital effect*; it is isotropic (3D) and thus distinctly different from the 2D conductance enhancement by the WL interference effects observed in the magnetically doped topological insulators[20]. It originates from the presence of disorder-induced localized spins[3] and, as witnessed by the characteristically non-analytic negative magnetoresistance (neg-MR), is governed by the distribution of very large spin g-factors that widens with decreasing localization length ξ in a way akin to an assembly of quantum wells[21].

RESULTS

Magnetotransport under strong disorder

The experiments were performed on 20-nm thin films of Sb_2Te_3, in which extreme positional disorder (amorphous state) is possible to obtain without finetuning the deposition parameters (Supplementary Note 1). Sb_2Te_3, in addition to being a canonical topological material[16] in a crystalline state, is also a well known phase-change material (PCM)[22] (Supplementary Fig. 1), that undergoes amorphous-to-crystalline transformation with the concurrent orders-of-magnitude resistive drop, and hence a huge

[1]Department of Physics, The City College of New York - CUNY, New York, NY 10031, USA. [2]Laboratoire des Solides Irradiés, École Polytechnique, CNRS, CEA, Université Paris-Saclay, 91128 Palaiseau cedex, France. [3]Helmholtz-Zentrum Berlin für Materialien und Energie, 12489 Berlin, Germany. ✉email: lkrusin@ccny.cuny.edu
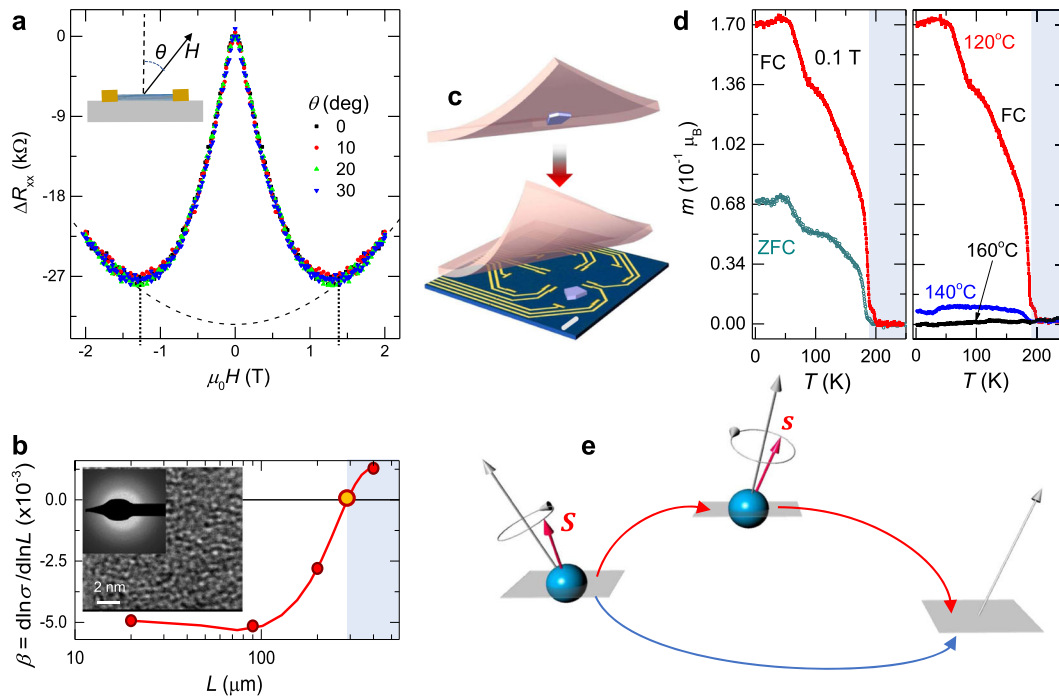
Fig. 1 Non-equilibrium spin correlations in strongly disordered Sb₂Te₃. a Longitudinal resistance $R_{xx}(H)$ of strongly disordered Sb_2Te_3 films ($T_a = 120\,°C$) does not depend on the tilt of magnetic field (see sketch). The dissipation reduction is relatively large (several %); it is observed below H_{max}, the field at which $\Delta R_{xx}(H)$ crosses over to the H^2-dependence (dash). Data in **a** were taken at 1.9 K. **b** As-deposited Sb_2Te_3 films are amorphous as seen by the transmission electron microscopy (inset). The lateral size L dependence of longitudinal conductivity σ obeys Anderson size scaling[1]; when Anderson parameter $\beta = dln\sigma/dlnL > 0$ the system is a 'metal' and when $\beta < 0$ it is an 'insulator'. **c** Thin (20 nm) Sb_2Te_3 flakes were exfoliated and transferred atop a μ-Hall sensor ("Methods"). The scale bar is 50 μm. **d** Magnetic moment per atom, m, measured by a μ-Hall sensor. Left: m in a 0.1 T field under field-cooling (FC) and zero-field-cooling (ZFC) conditions. Right: m of the same flake for three levels of disorder indexed by T_a. It onsets at ~200 K, saturates at low T, and becomes vanishingly small for $T_a \gtrsim 160\,°C$. **e** Cartoon of electron hopping to a distant empty site under flowing current, see text. The electron with spin S may reach this site directly or via an intermediate site hosting localized spin s. Random disorder landscape induces spatial randomness in the spin g-factors and hence the randomness of local fields (gray arrows) controlling the precession of all spins. The indirect channel will depend on the state of s during hopping attempts and the memory of this state is encoded in the transport of charge. These spin correlations are destroyed by magnetic field, and consequently the resistance is reduced.

range of disorder and its effect on the topological properties could be controllably explored.

Our first key finding is shown in Fig. 1a. The change in the longitudinal magnetoresistance ΔR_{xx} in the amorphous Sb_2Te_3 films at low magnetic fields is with a remarkable fidelity impervious to the tilt of magnetic field. It is relatively large and negative (i.e., charge transport becomes less dissipative with increasing field) up to a field H_{max} (Fig. 1a and Supplementary Fig. 2). The as-deposited films are highly resistive and obey Anderson scaling[1] (Fig. 1b) consistent with electron localization (Supplementary Note 2), which can be induced either by increasing system size for fixed disorder or decreasing disorder for fixed system size. Robust in 3D, such scaling is marginal in 2D unless there is a strong SOC, hence a 2D localization in our thin films is not precluded. The field isotropy of the low-field dissipation 'quench' naturally suggests a spin-dominated 3D mechanism rather than orbital effect, and so the pertinent question to ask is how such behavior can proceed in a system where electronic states are localized and the *extrinsic* spinfull impurities are absent (see Supplementary Table 1).

Direct detection of 'glassy' magnetic signal

To start we note that in the presence of disorder a finite population of singly occupied states below the Fermi energy E_F has been discussed as long as 20 years back by Sir Neville Mott[3]. Magnetic response from randomly localized spins in such 'Fermi glass' state was expected to be weak and, as far as we know, has never been experimentally demonstrated. So our second

surprising finding was a very robust magnetic signal from the disordered Sb_2Te_3 films directly detected using a custom-designed μHall sensors (Fig. 1c, d), with the thin film flakes mechanically exfoliated from their substrates and transferred onto the active sensor area ("Methods", Supplementary Fig. 3, Supplementary Note 4). We surmise that here the observed effective moment per atom is significantly amplified by the large effective Landé g-factor[4] in Sb_2Te_3, where SOC is strong[16]. The detected signal depends on the magnetic history (field-cooling vs. zero-field cooling), which, together with slow magnetic relaxation (Supplementary Fig. 3c) reflects a glassy nature of the localized state. We emphasize that magnetic signal crucially depends on the level of disorder; indeed, it becomes barely detectable in the crystalline phase as disorder in *the same film* is reduced by thermal annealing (Fig. 1d).

Spin memory effect

Under strong disorder charge transport is a complex electron hopping process that at low temperatures proceeds via quantum tunneling between localized states assisted by phonons[10,19]. While considerations of magnetotransport have mainly focused on the orbital effects, a recently proposed idea[18] takes note of putative nonequilibrium spin correlations in the localized regime created by the flowing current when electron hopping times τ are short relative to the spin relaxation times τ_s. These time scales determine the magnetic field range over which spin-correlation-driven neg-MR (positive magnetoconductance) ought to be present.
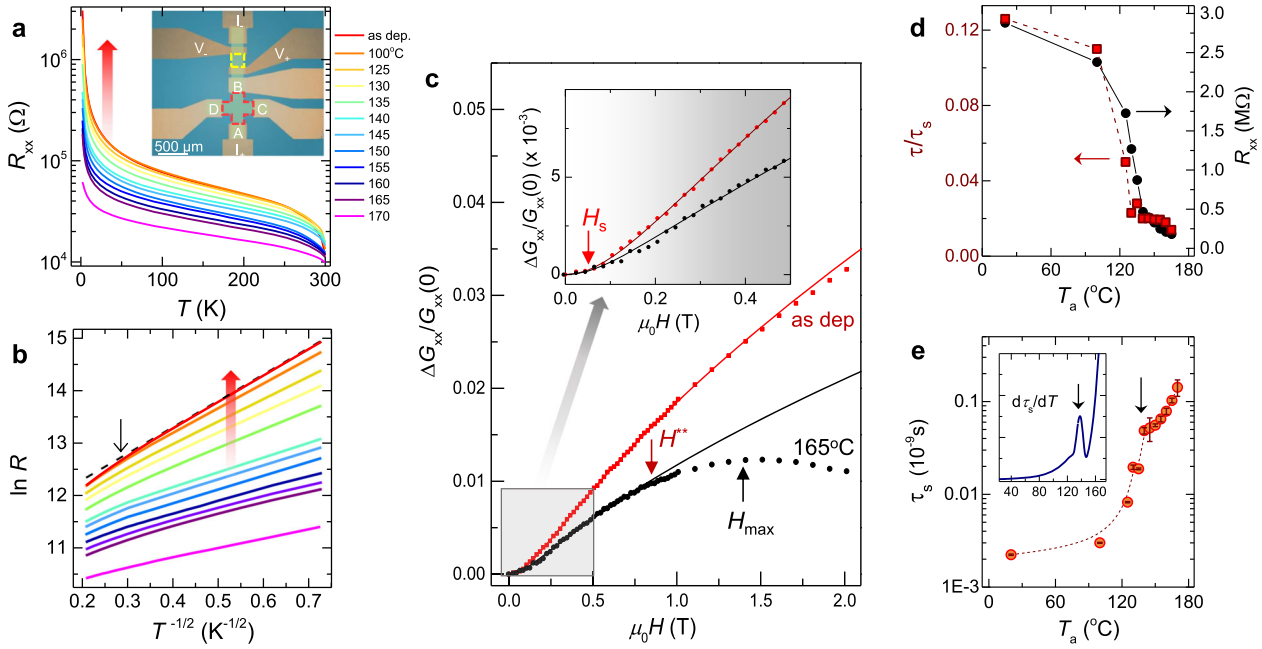
Fig. 2 Spin memory effect in the longitudinal conductance G_{xx} of Sb_2Te_3 in the VRH regime. a $R_{xx}(T)$ of a 20 nm thin Sb_2Te_3 film under strong disorder increases at low temperatures by orders of magnitude; the strength of disorder is reproducibly controlled by T_a. Inset: lithographically patterned Hall-bar and van der Pauw contact configurations used in measurements of R_{xx}. **b** R_{xx} exponential in inverse $\sqrt{T}$ confirms that below ~10 K (black down-arrow) charge transport is by the 3D VRH[19], the regime where dynamic spin correlation are expected. The color code is as in **a**. Red arrows in **a** and **b** point in the direction of increasing disorder. **c** Field dependence of G_{xx} for two disorder states shown at 1.9 K. A fit (solid lines) to Eq. (1) fully reproduces the non-analytic form of $\Delta G_{xx}(H)/G_{xx}(0)$ arising from spin-memory in the VRH regime. Inset: Zoom of the data at low fields. **d** Disorder dependence of τ/τ_s, the ratio of hopping to spin-relaxation time, is found to closely correlate with the low-T R_{xx}. **e** τ_s increases by nearly two orders of magnitude in the disorder range studied; it is a very sensitive probe of the phase change at crystallization, see inset.

The idea is illustrated in Fig. 1e. When the current is injected, an electron with spin S attempting to hop to an available empty site can do it in two ways: directly or via an intermediate site occupied by a localized spin s. It may take several attempts for the indirect hops to succeed and the return probability will depend on history, i.e., on whether the tunneling electron can form a triplet or a singlet state with s. For example, in the absence of disorder a triplet state would remain so in the presence of applied magnetic field and no reduction of magnetoresistance (increase of magnetoconductance) is expected. Under strong disorder (such as shown in Fig. 1b), however, spin g-factors will be spatially random so that localized spins at different sites will precess incoherently and spin correlations will be destroyed by the field. Accordingly, in a simple model[18] the change in magnetoconductance ΔG_{xx} arising from such spin correlations should follow not a power law[25] but a unique non-analytic form:

$$\frac{\Delta G_{xx}(H)}{G_{xx}(0)} \sim A \left[-\Gamma\left(-\frac{d_s}{2}\right) \right] \sum_{l=-1}^{1} \left[\left(\frac{ilH}{H^{\star\star}} + \frac{\tau}{\tau_s} \right)^{d_s/2} - \left(\frac{\tau}{\tau_s} \right)^{d_s/2} \right],$$

(1)

where $A = \frac{G_{xx}(H \to \infty) - G_{xx}(0)}{G_{xx}(0)}$, $d_s = 4/3$ is the spectral dimension of the percolation cluster[26] (which is the relevant dimension in the hopping process), l is an index for the diffusing spin, $\Gamma(-\frac{d_s}{2})$ is the gamma function $\cong -4$, and $H^{\star\star} = \frac{\hbar}{\mu_B \tau \Delta g}$ is the limiting magnetic field range set by the hopping rate $1/\tau$ and the disorder-induced spread Δg of spin g-factors.

The strongly localizing behavior we observe in the longitudinal resistance R_{xx} (Fig. 2a) at low temperatures (below ~10 K) follows variable range hopping (VRH) law $R_{xx}(T) = R_0 \exp\left(\frac{T_0}{T}\right)^{1/2}$ of Efros-Shklovskii (E-S) kind[10], see Fig. 2b. The E-S energy scale T_0 characteristic of the hopping process (Supplementary Fig. 1b) is tracked on decreasing disorder by a well controlled thermal annealing schedule ("Methods"); it is inversely proportional to the

electron localization length[19] ξ, which we will show controls the g-factor distribution width Δg. We remark that in this regime (at low T) the detected magnetic moment appears 'flat' in temperature (Fig. 1d).

In the VRH regime, the fit of conductance to Eq. (1) for two states of disorder is illustrated in Fig. 2c. As seen in the figure, at low magnetic fields the characteristic non-analytic behavior is accurately followed; here the ratio of hopping time to spin relaxation time τ/τ_s and the hopping field scale $H^{\star\star}$ were used as fitting parameters ("Methods"). The fits at different disorder levels controlled by the anneals at different temperatures T_a are shown in Supplementary Fig. 4. The ratio τ/τ_s strongly depends on the level of disorder (Fig. 2d), with the hopping and spin relaxation rates, $1/\tau \propto H^{\star\star}$ and $1/\tau_s \propto H_s$, in close correspondence with the disorder dependence of R_{xx} all the way through crystallization transition. The hopping time τ can be independently extracted from the E-S energy (Supplementary Fig. 5a), and, as expected for the hopping conductivity τ increases exponentially on decreasing temperature (Supplementary Fig. 5b). This allows us to consistently obtain the evolution of spin-relaxation time τ_s (Fig. 2e) and Δg (Fig. 3a) with decreasing disorder (increasing T_a), and hence that of the low-field spin-relaxation scale $H_s = \frac{\hbar}{\mu_B \tau_s \Delta g}$ (Supplementary Fig. 6); H_s marks a crossover from the concave-up field shape associated with τ_s to concave-down behavior at higher fields, see Fig. 2c.

An intriguing question arises as to what controls the unexpectedly large (Tesla-range) field scale where neg-MR, the hallmark of dynamic spin memory, is found. For the systems with small spin-orbit coupling where g-factor ~2, the expected field range would be in the 10^{-4}–10^{-5} Tesla range. In theory[18], this range is set by the competition between the magnetic energy $g\mu_B H$ and either thermal energy or the exchange J between neighboring spins—it ought to be well below the competing
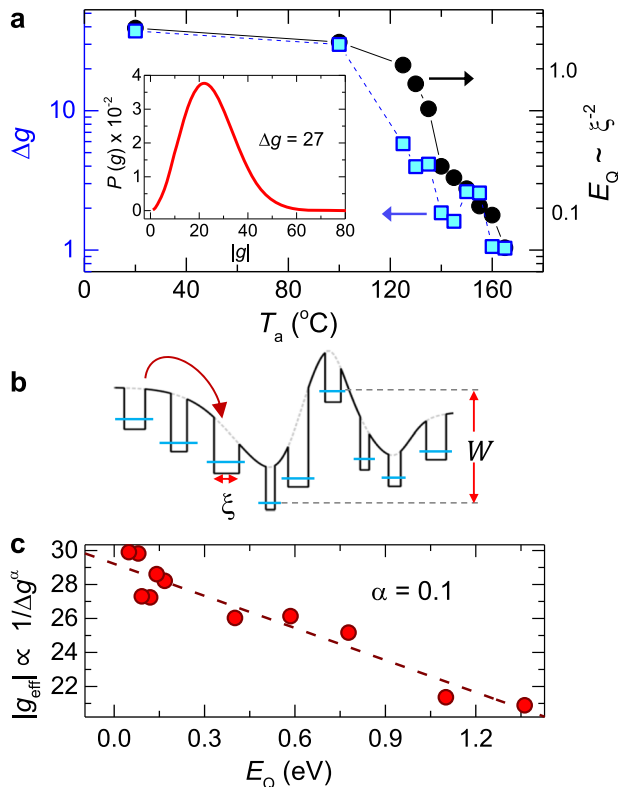
Fig. 3 Distribution of spin g-factors and confinement energy. a Width Δg of the g-factor distribution $P(g)$ vs. T_a follows the confinement energy $E_Q(T_a)$. E_Q is modeled by a particle-in-a-box and calculated using ξ as a box size. In the amorphous state in the conduction tail states effective mass is strongly enhanced[23]. Inset: $P(g)$ calculated in the strong SOC regime[24] for $\Delta g = 27$. **b** A model of disorder landscape within the Anderson bandwidth W riding on a long-range smooth potential[10]. **c** Effective g-factor, $|g_{eff}|$, increases with E_Q. We note that the sign of g for many semiconductors, particularly with strong SOC, is negative[4].

effects. Here, however, with large effective g value[27], $g\mu_B H/k_B$ ~ 20 K is comparable to the spin-memory range. This brings us back to disorder-induced spin correlations. Fig. 1d shows that under extreme disorder the onset of magnetic response is rather abrupt and at a remarkably high temperature T_s ~200 K. While the details of spin correlations in this Anderson-like-localized glassy state clearly deserve further experimental and theoretical studies, a rough estimate of $J \sim k_B T_s/z \approx 70$ K, using local coordination number[22] z ~3 expected in Sb_2Te_3, implies that here short range interactions between localized spins play the key role.

Large fluctuations of Landé g-factors

Let us now consider g-factor fluctuations in a strongly disordered state. The g distribution width naturally arising from our magnetoconductance data (Fig. 3a) within the model considered above is spectacularly wide at the highest level of disorder, $\Delta g \simeq 40$; it exceeds the effective g value of ~30 obtained, e.g., directly in the same topological insulator family from the electron spin resonance (ESR) experiments[27]. Such large g spread is uncommon but not unprecedented. Giant fluctuations of g-factors have been reported in, e.g., InAs nanowires where $\Delta g > |g_{eff}|$ and the effective factor $|g_{eff}|$ is also large[24]. Furthermore, in semiconducting quantum wells $|g_{eff}|$ has been known to increase roughly linearly[21] with quantum confinement energy E_Q as $|g_{eff}| \simeq g_0 + \beta E_Q$, where β is a material-specific constant. Here we propose that in the strongly localized state (Supplementary Note 2), quantum confinement is enforced by the wells constrained by the

localization length ξ (Fig. 3b). In this view, a simple particle-in-a-box approximation gives $E_Q \propto \xi^{-2}$ that indeed fully scales with Δg (Fig. 3a). The expected linear $|g_{eff}|$ vs. E_Q would then set $|g_{eff}| \sim \Delta g^{-\alpha}$ with $\alpha \sim 0.1$, with $|g_{eff}|$ approaching the ESR-determined value in the unconfined state, see Fig. 3c.

Mapping spin memory phase space

Our experiments reveal how positive $\Delta G_{xx}(H)$ (neg-MR) evolves with decreasing disorder; it persists over a spectacularly large disorder range, all the way through the crystallization process and beyond (Fig. 4a). The large limiting field range set by H_{max} at strong disorder falls with increasing T_a (Fig. 4b) to pinch off $\Delta G_{xx}(H)$ eventually to null. A clear visual of the field-disorder phase space is shown in Fig. 4c, where the strength of disorder is represented by E_Q. $H - E_Q$ diagram shows that spin-memory region is restricted by $H^{\star\star}$ to relatively low fields, but when the system is less localized the 'envelope' of the spin-memory space switches to H_{max}.

The temperature range over which spin memory is evident is set by the VRH process (Fig. 2b), with $\Delta G_{xx}(H)$ well described by Eq. (1). Above ~10 K, outside the VRH region, $\Delta G_{xx}(H)$ becomes nearly 'flat' (Fig. 4d); there both τ_s (Supplementary Fig. 7a) and $|g_{eff}|$ (see Supplementary Fig. 7b) appear to saturate, and spin-memory phenomenon is not expected. The typical field scale associated with the E-S energy T_0 ~ 10–30 K is in the 1–2 T range, in close correspondence with $H^{\star\star}$ at low T. As before, $H_{max} H^{\star\star}$, and in the low-temperature localized state H_{max} becomes the limiting crossover field (Fig. 4e). Above $T_a \simeq 180$ °C ($E_Q \approx 60$ meV), in the strongly disordered *crystalline* state spin memory phenomenon is not detectable.

Transition to a 2D weak antilocalization regime

The exit from the spin-memory state at $\cong 180$ °C is clearly evidenced by a transition from the negative MR (neg-MR) to a positive MR (pos-MR) 'cusp' characteristic of the WAL state (Fig. 5a). The WAL cusp[29] scales with the transverse component of applied magnetic field $H_\perp = H \cos \theta$ (Fig. 5b), consistent with the 2D (orbital) character expected in a topological insulator[8] under weak disorder. This 2D scaling should be contrasted with isotropic (3D) scaling of the neg-MR peak in the spin-memory state. Thus, unlike the WL-WAL transition driven by magnetic impurities[20], the transition from spin-memory onto a WAL state is also a 3D-2D dimensionality transition at which the electron system rapidly delocalizes. We remark again that WAL onsets at $\simeq 180$ °C, way above the crystallization temperature of $\simeq 140$ °C (see inset in Fig. 5c), pointing to a disorder threshold for the gapless topological state.

DISCUSSION

The emergence of WAL in the diffusive transport regime[3] should be reflected in the evolution of the electron localization length ξ. Figure 5c shows that with increasing T_a, ξ first experiences a 'kink' at the first order crystallization transition[22]. However, its largest change—an increase by orders of magnitude—initiates at the onset of WAL. We note that the electron mean free path is only limited by the film thickness and the grain size in the crystalline state at high T_a (Supplementary Fig. 8).

To translate T_a into a disorder energy scale W_D[12] we use the annealing evolution of the full-width-half-max (FWHM) of the in-plane Raman E_G^2 mode (Fig. 5c and Supplementary Fig. 1) as a metric of disorder[30]. A simple phenomenological scaling is derived by setting maximum disorder in the amorphous state at the energy corresponding to the bulk gap E_G ~200 meV[16] in the crystalline state and minimum disorder (at the highest T_a) to zero (Fig. 5d, Supplementary Note 11, and Supplementary Fig. 9). When the angular field-dependence of magnetoresistance ΔR is plotted
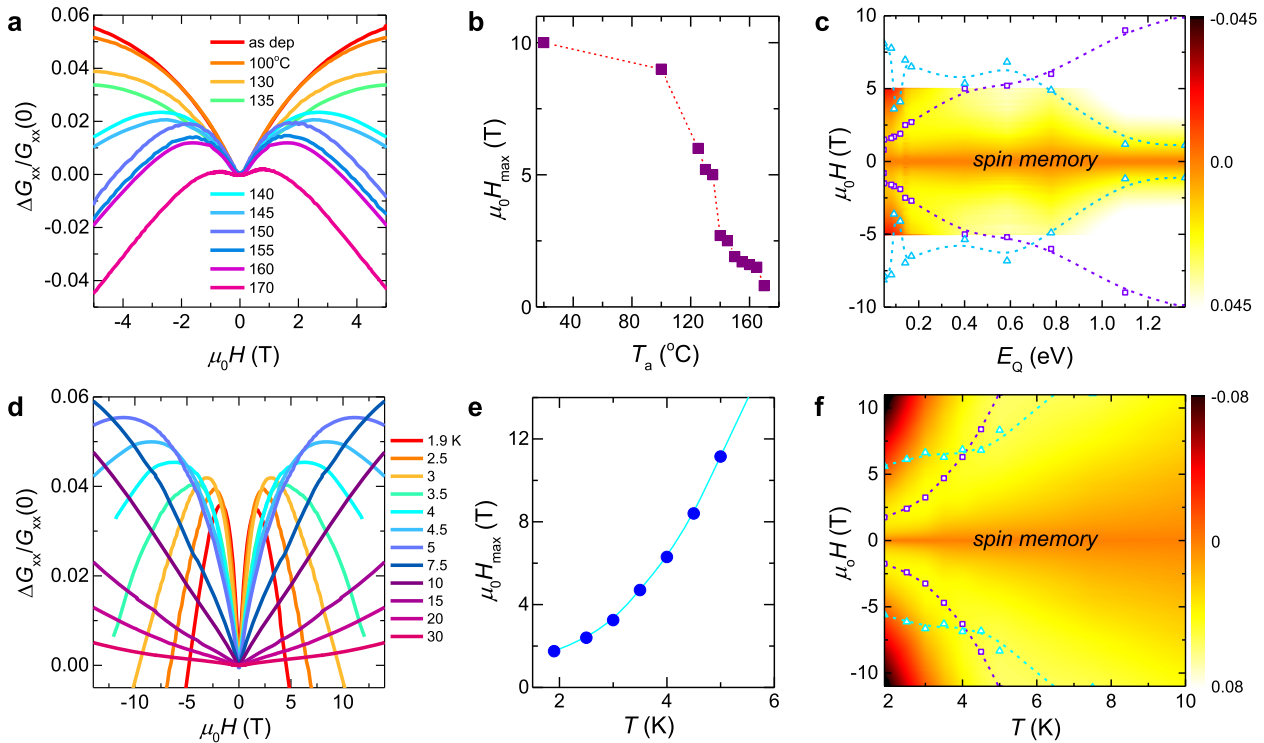
Fig. 4 Phase diagrams of the spin-memory state. a Normalized change in $\Delta G_{xx}(H)/G_{xx}(0)$ at 1.9 K for different levels of disorder labeled by T_a. At low disorder the non-analytic positive spin-memory `cusp' transforms into a parabolic form when the huge conductance rise near crystallization is nearly complete. **b** The transformation occurs via reduction of the crossover field H_{max}. **c** Phase diagram in the $H - E_Q$ space showing the huge disorder range where spin memory effect is present. **d** $\Delta G_{xx}(H)/G_{xx}(0)$ shown for $T_a = 150$ °C at different bath temperatures T. As T increases the spin-memory `cusp' grows and widens until the system exits the VRH regime and enters the regime where transport eventually becomes diffusive. **e** In the VRH range the crossover field H_{max} monotonically increases with T. **f** Phase diagram in the $H - T$ space controlled by spin memory. At low T this range is bounded by $H_{max} \lesssim H^{**}$. The color scales of the contour plots indicate the level of $\Delta G_{xx}(H)/G_{xx}(0)$. H_{max} (hollow purple squares) and the hopping field scale H^{**} (hollow blue triangles) combine to define a limiting envelope for the spin-memory space.

as a function of W_D (Fig. 5d), the 3D-2D transition from the spin-memory state to WAL at a surprisingly low ($W_D^{2D} \sim 10$ meV) disorder level is strikingly apparent. Figure 5e shows that at W_D^{2D} the low-temperature longitudinal conductance G_{xx} is with good precision equal to one conductance quantum $G_0 = \frac{e^2}{h}$. This suggests that at the transition only one topological channel is present. To test this we fit the field dependence of the WAL conductance to 2D localization theory[28] of Hikami, Larkin and Nagaoka (HLN)

$$\Delta G_{xx}(B) \simeq a\frac{e^2}{2\pi^2\hbar}f\left(\frac{B_\phi}{B}\right),\qquad(2)$$

where $f(x) \equiv \ln x - \psi(1/2 + x)$, ψ is the digamma function, and field $B_\phi = \frac{\hbar}{4el_\phi^2}$ is related to the dephasing length l_ϕ of interfering electron paths (Supplementary Note 12, Supplementary Fig. 10). The number n_Q of quantum conduction channels contributing to WAL can be estimated from the coefficient $a = n_Q/2$, which equals to 1/2 for a single 2D channel. The plot of a (insert in Fig. 5e) indeed confirms that maximum $a \cong 1/2$ is at $T_a \cong 180$ °C corresponding to W_D^{2D} (see Supplementary Fig. 10a). The decrease of a at lower disorder is likely due to increased conductivity of the 2D electron gas states of bulk origin[11].

To summarize, we directly detect a glassy spin response from thin films of Sb_2Te_3 under strong structural disorder, which vanishes in the same film when disorder is sufficiently reduced. Under strong disorder, the system develops spin-correlations that drive the spin-memory phenomenon controlling the transport of charge, with the key features well captured by a simple phenomenology. Both in magnetic field and in disorder strength, the parameter space where spin memory exists is unexpectedly

broad—it persists well into a disordered crystalline state where, eventually, a 2D WAL quantum interference correction is recovered. We remark that in Sb_2Te_3 electron correlations at the transition are weak in the Mott sense[3]; taking the carrier density $n \lesssim 10^{20}$ cm^{-3} (Supplementary Fig. 8b) and Bohr radius $a_B \sim 60$ nm[31] we obtain $n^{1/3}a_B \simeq 28$, more than ~100 times the Mott criterion of 0.25. Strong charge screening in Sb_2Te_3 (large dielectric constant $\epsilon \sim 170$[31]) renders the Coulomb energy ($E_C \simeq 4$ meV) much smaller than the Fermi energy ($E_F \simeq 260$ meV); with $E_C \ll E_F$ this points to the transition to be disorder-driven[32].

Our findings show that spin-memory effect sets a disorder threshold at which topological protection of the surface states is reclaimed, although bulk channels may still contribute. Direct measurements of glassy spin response in materials other than Sb_2Te_3 are yet to be carried out; it is clear, however, that for spin memory the spin-lifetime τ_s has to be much longer than the hopping time τ. We expect spin memory to be visible in a broader family of strong SOC materials; it has been reported in $SnSb_2Te_4$[33], where crystal (and defect) structure is different[34]. The electrical control of this spin-dependent transport can, in principle, be achieved through electrostatic gating[35], and by locally modifying spin correlations using currently practiced doping techniques.

METHODS

Film growth and structural characterization
Films of Sb_2Te_3 with thicknesses ranging from 20 to 100 nm were sputter-deposited at room temperature in Ar gas at 4 mTorr and a flow of 46 sccm from a nominally stoichiometric target using 15 W DC power on Si_3N_4 (100 nm)/Si substrates. The stoichiometry was confirmed by Rutherford
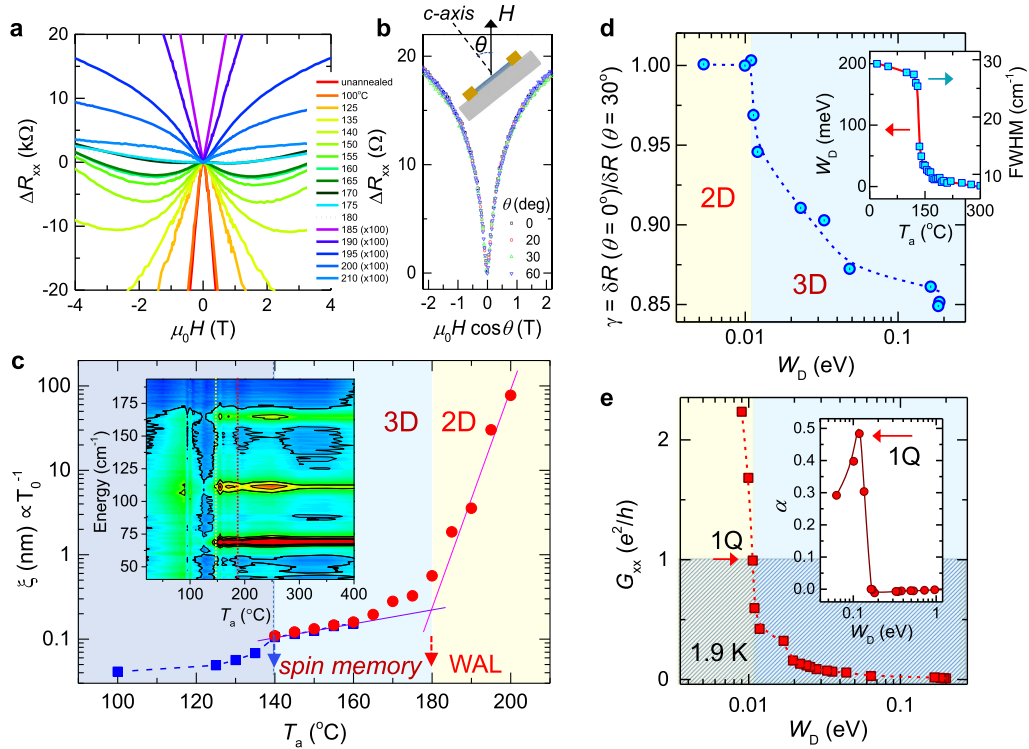
Fig. 5 Transition from the spin-memory to weak antilocalization (WAL) state in disordered crystalline Sb$_2$Te$_3$ films. a Upon annealing, ΔR_{xx} undergoes transition from the spin memory neg-MR state to a positive magnetoresistance (pos-MR) WAL regime at $T_a \cong 180\,°C$, when charge transport becomes diffusive. **b** The WAL pos-MR has a 2D character as evidenced by the scaling with the transverse component of magnetic field. **c** Localization length $\xi \propto T_0^{-1}$ shows a distinct kink at crystallization and a smooth transition to a 2D WAL state. T_0 was obtained from fitting to the E-S VRH formula[10]. Inset: Crystallization at $T_a \cong 140\,°C$ (yellow dash) is clearly seen as sharp lines in the Raman spectra vs.T_a. Transition to WAL at $\simeq 180\,°C$ is indicated by red dash. **d** Ratio γ of low-field δR with the magnetic field out-of-plane ($\theta = 0$) to the one with a field tilt $\theta = 30°$ vs. disorder parameter W_D. In the 2D WAL regime γ is constant, owing to scaling with $H_\perp = H\cos\theta$. Inset: W_D is obtained from parametric scaling of the FWHM vs. T_a of E_G^2 in-plane Raman mode (see Supplementary Note 11). **e** Longitudinal conductance G_{xx}vs.W_D. $G_{xx} \cong e^2/h$ at the transition to 2D WAL. Inset: The number of quantum channels estimated from the fit to HLN theory[28]. At the transition parameter $a \approx 0.5$ indicates a single quantum channel.

Backscattering (RBS) and particle induced X-ray emission (PIXE). RBS data were collected at NEC 3UH Pelletron using a Si surface barrier detector with He$^+$ ions at 2.3 MeV. PIXE data was collected using a Si-Li detector with H$^+$ ions at 1 MeV. Elemental analysis was done at Evans Analytical Group. X-ray diffraction characterization was performed using Bruker D8 Discover system with the da Vinci configuration using a monochromated beam ($\lambda_{Cu} = 1.5418\,Å$) and a scintillator detector with analyzer crystal (HR-XRD). The film morphology was characterized using the FEI Titan Themis 200 transmission electron microscope (TEM), 200 kV, with TEM resolution 0.9 Å and 4 k × 4 k Ceta 16 M CMOS camera. Disorder was characterized by Raman spectra using 633 nm linearly polarized excitation in a back-scattering configuration[30], with power kept below 2 mW to avoid heating effects.

Magnetic measurements
Magnetic measurements were performed using custom-designed on-chip μ-Hall sensors based on In$_{0.15}$Ga$_{0.85}$As heterostructures (SI). To measure magnetization, ~50 μm in lateral size thin Sb$_2$Te$_3$ film samples were exfoliated from their substrates and placed directly on the SiO$_2$-passivated sensor using PDMS. At each temperature an empty twin sensor was used for background subtraction.

Transport measurements
Transport measurements were performed in a 14 Tesla Quantum Design PPMS system in 1 mTorr of He gas on many film samples, each subjected to the same annealing protocol used to tune the level of disorder. Lithographically patterned structures combining both Hall bar and van der Pauw electrical contact configurations with Ti/Au metallurgy were used (Fig. 2a). Measurements were performed on as-deposited films and on the same films after each 5 min annealing step in a box furnace in

flowing nitrogen in the temperature range across crystallization at $T_a \sim 140\,°C$. We used a numerical Monte Carlo technique to fit our transport data to Eq. (1).

REFERENCES
1. Abrahams, E., Anderson, P., Licciardello, D. & Ramakrishnan, T. Scaling theory of localization: absence of quantum diffusion in two dimensions. *Phys. Rev. Lett.* **42**, 673–676 (1979).
2. Evers, F. & Mirlin, A. Anderson transitions. *Rev. Mod. Phys.* **80**, 1355–1417 (2008).
3. Mott, N. *Metal-insulator Transitions* (Taylor & Francis, New York, 1997).
4. Winkler, R. *Spin-Orbit Coupling Effects in Two-dimensional Electron and Hole Systems* (Springer-Verlag, Berlin-Heidelberg-New York, 2003).
5. Žutić, I., Fabian, J. & DasSarma, S. Spintronics: fundamentals and applications. *Rev. Mod. Phys.* **76**, 323–410 (2004).
6. Qi, X.-L. & Zhang, S.-C. Topological insulators and superconductors. *Rev. Mod. Phys.* **83**, 1057–1110 (2011).
7. Scanlon, D. et al. Controlling bulk conductivity in topological insulators: key role of anti-site defects. *Adv. Mater.* **24**, 2154–2158 (2012).
8. Zhao, L. et al. Stable topological insulators achieved using high energy electron beams. *Nat. Comm.* **7**, 10957 (2016).

9. Beidenkopf, H. et al. Spatial fluctuations of helical Dirac fermions on the surface of topological insulators. *Nat. Phys.* **7**, 939–943 (2011).
10. Gantmakher, V. *In Electrons and Disorder in Solids* (Clarendon Press, Oxford, 2005).
11. Zhang, L. et al. Weak localization effects as evidence for bulk quantization in Bi_2Se_3 thin films. *Phys. Rev. B* **88**, 121103 (2013).
12. Li, J., Chu, R.-L., Jain, J. & Shen, S.-Q. Topological Anderson insulator. *Phys. Rev. Lett.* **102**, 136806 (2009).
13. Groth, C., Wimmer, M., Akhmerov, A., Tworzydło, J. & Beenakker, C. Theory of the topological Anderson insulator. *Phys. Rev. Lett.* **103**, 196805 (2009).
14. Guo, H.-M., Rosenberg, G., Refael, G. & Franz, M. Topological Anderson insulator in three dimensions. *Phys. Rev. Lett.* **105**, 216601 (2010).
15. Mitchell, N. P., Nash, L. M., Hexner, D., Turner, A. M. & Irvine, W. T. M. Amorphous topological insulators constructed from random point sets. *Nat. Phys.* **14**, 380–385 (2018).
16. Zhang, H. et al. Topological insulators in Bi_2Se_3, Bi_2Te_3, and Sb_2Te_3 with a single Dirac cone on the surface. *Nat. Phys.* **5**, 438–442 (2009).
17. Zhao, L. et al. Singular robust room-temperature spin response from topological Dirac fermions. *Nat. Mater.* **13**, 580–585 (2014).
18. Agam, O., Aleiner, I. & Spivak, B. Spin-memory effect and negative magnetoresistance in hopping conductivity. *Phys. Rev. B* **89**, 100201 (2014).
19. Shklovskii, B. & Efros, A. *Electronic Properties of Doped Semiconductors* (Springer-Verlag, Berlin, 1984).
20. Liu, M. et al. Crossover between weak antilocalization and weak localization in a magnetically doped topological insulator. *Phys. Rev. Lett.* **108**, 036805 (2012).
21. Chen, Z., Carter, S., Bratschitsch, R., Dawson, P. & Cundiff, S. Effects of disorder on electron spin dynamics in a semiconductor quantum well. *Nat. Phys.* **3**, 265–269 (2007).
22. Shakhvorostov, D. et al. Evidence for electronic gap-driven metal-semiconductor transition in phase-change materials. *Proc. Natl Acad. Sci. USA* **106**, 10907–10911 (2009).
23. Singh, J. Effective mass of charge carriers in amorphous semiconductors and its applications. *J. Non-Cryst. Solids* **299-302**, 444–448 (2002).
24. Csonka, S. et al. Giant fluctuations and gate control of the g-factor in InAs nanowire quantum dots. *Nano Lett.* **8**, 3932–3935 (2008).
25. Ioffe, L. & Spivak, B. Giant magnetoresistance in the variable-range hopping regime. *J. Exp. Theor. Phys.* **117**, 551–569 (2013).
26. Havlin, S. & Ben-Avraham, D. Diffusion in disordered media. *Adv. Phys.* **51**, 187–292 (2002).
27. Woloś, A. et al. g-factors of conduction electrons and holes in Bi_2Se_3 three-dimensional topological insulator. *Phys. Rev. B* **93**, 155114 (2016).
28. Hikami, S., Larkin, A. & Nagaoka, Y. Spin-orbit interaction and magnetoresistance in the two-dimensional random system. *Prog. Theor. Phys.* **63**, 707–710 (1980).
29. Garate, I. & Glazman, L. Weak localization and antilocalization in topological insulator thin films with coherent bulk-surface coupling. *Phys. Rev. B* **86**, 035422 (2012).
30. Secor, J. et al. Phonon renormalization and Raman spectral evolution through amorphous to crystalline transitions in Sb_2Te_3 thin films. *Appl. Phys. Lett.* **104**, 221908 (2014).
31. Heremans, J., Cava, R. & Samarth, N. Tetradymites as thermoelectrics and topological insulators. *Nat. Rev. Mater.* **2**, 17049 (2017).
32. Siegrist, T. et al. Disorder-induced localization in crystalline phase-change materials. *Nat. Mater.* **10**, 202–208 (2011).
33. Reindl, J., Volker, H., Breznay, N. & Wuttig, M. Persistence of spin memory in a crystalline, insulating phase-change material. *npj Quantum Mater.* **4**, 57 (2019).
34. Menshchikova, T., Eremeev, S. & Chulkov, E. Electronic structure of $SnSb_2Te_4$ and $PbSb_2Te_4$ topological insulators. *Appl. Surf. Sci.* **267**, 1–3 (2013).
35. Sandhu, J., Heberle, A., Baumberg, J. & Cleaver, J. Gateable suppression of spin relaxation in semiconductors. *Phys. Rev. Lett.* **86**, 2150–2153 (2001).

ACKNOWLEDGEMENTS

AUTHOR CONTRIBUTIONS

Experiments were designed by L.K.-E., I.K., and S.R. grew Sb_2Te_3 films. I.K. performed structural characterization. I.K., L.Z., and Z.C. fabricated devices for transport measurements performed by I.K., H.D., and Z.C. M.K. designed Hall-sensors for magnetic measurements performed by L.Z. and S.Z. Data analysis was done by I.K., H.D., L.Z., Y. D., and L.K.-E. L.K.-E. wrote the manuscript with input from I.K., H.D., and L.Z.

COMPETING INTERESTS

The authors declare no competing interests.

ADDITIONAL INFORMATION

Supplementary information is available for this paper at https://doi.org/10.1038/s41535-020-0241-5.

Correspondence and requests for materials should be addressed to L.K.-E.

Reprints and permission information is available at http://www.nature.com/reprints

Publisher's note Springer Nature remains neutral with regard to jurisdictional claims in published maps and institutional affiliations.